Inorganic Chemistry

Article

pubs.acs.org/IC

Spontaneous Redox Synthesis of the Charge Transfer Material $TTF_4[SVMo_{11}O_{40}]$

Qi Li,[†] Jinzhen Lu,[†] John F. Boas,[§] Daouda A. K. Traore,[∥] Matthew C. J. Wilce,[∥] Fuzhi Huang,[⊥] Lisandra L. Martin,[†] Tadaharu Ueda,*[,‡] and Alan M. Bond*[,†]

[†]School of Chemistry, Monash University, Clayton, Victoria 3800, Australia

[‡]Department of Applied Science, Faculty of Science, Kochi University, Japan

[§]School of Physics, Monash University, Clayton, Victoria 3800, Australia

[∥]Department of Biochemistry and Molecular Biology, Monash University, Clayton, Victoria 3800, Australia

[⊥]Department of Materials Engineering, Monash University, Clayton, Victoria 3800, Australia

Supporting Information

ABSTRACT: The charge-transfer material TTF-$SV^{IV}Mo_{11}O_{40}$ (TTF = tetrathiafulvalene) was prepared by a spontaneous redox reaction between TTF and the vanadium-substituted polyoxometalate $(n\text{-}Bu_4N)_3[SV^{V}Mo_{11}O_{40}]$ in both solution and solid state phases. Single crystal X-ray diffraction gave the stoichiometry $TTF_4[SVMo_{11}O_{40}]\cdot 2H_2O\cdot 2CH_2Cl_2$, with the single V atom positionally disordered with eight Mo atoms over the whole α-Keggin polyanion $[SVMo_{11}O_{40}]^{4-}$. Raman spectra support the 1+ charge assigned to the oxidized TTF deduced from bond lengths, and elemental and voltammetric analysis also are consistent with this formulation. Scanning electron microscopy images showed a rod-type morphology for the new charge-transfer material. The conductivity of the solid at room temperature is in the semiconducting range. The TTF and $(n\text{-}Bu_4N)_3[SV^{V}Mo_{11}O_{40}]$ solids also undergo a rapid interfacial reaction, as is the case with TTF and TCNQ (TCNQ = tetracyanoquinodimethane) solids. EPR spectra at temperatures down to 2.6 K confirm the presence of two paramagnetic species, V(IV) and the oxidized TTF radical. Spectral evidence shows that the TTF-$SV^{IV}Mo_{11}O_{40}$ materials prepared from either solution or solid state reactions are equivalent. The newly isolated TTF-$SV^{IV}Mo_{11}O_{40}$ material represents a new class of TTF-polyoxometalate compound having dual electrical and magnetic functionality derived from both the cationic and anionic components.

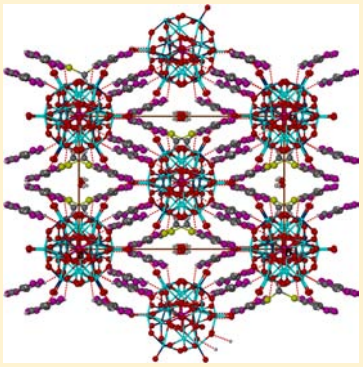

INTRODUCTION

Charge-transfer materials, which are composed of an electron donor and an electron acceptor, have attracted considerable attention due to their versatile electronic functionalities which result from the ground-state electron transfer between donor and acceptor moieties. Following the synthesis of the electron donor tetrathiafulvalene (TTF)[1,2] it was soon discovered that the combination of TTF and the electron acceptor tetracyanoquinodimethane (TCNQ) formed the charge-transfer complex TTF-TCNQ[3,4] which exhibited remarkable properties. For example, crystalline TTF-TCNQ exhibits one-dimensional metallic conductivity down to 54 K and hence became the first reported organic metal.[5] The fact that, in the solid state, reaction of TTF with TCNQ is rapid facilitated studies of the interfacial chemistry between these two solids.[6−9] Recently, metallic conductivity was reported at the interface between the two insulating TTF and TCNQ crystals if they were in direct mechanical contact,[6,7] which in turn generated a new research direction of interfacial phenomena for charge-transfer complexes. In particular, the formation of TTF-TCNQ nanowires was found in the interfacial reaction between aqueous TTF and TCNQ microparticles.[8]

The discovery of the metallic TTF-TCNQ complex was followed by the synthesis of other charge-transfer complexes derived from TTF that have demonstrated properties associated with semiconductors, metals, and even superconductors.[5] A goal in this area of research is to develop bifunctional materials that combine properties not normally associated with a monofunctional material. Materials based on the combination of TTF and a polyoxometalate (POM) represent one such class that could display interesting properties. Polyoxometalate anions are large inorganic clusters that have rich redox chemistry, electronic versatility, magnetism, and photochemistry.[10−15] These properties make them attractive building blocks for multifunctional hybrid materials. Consequently, hybrid TTF-POM charge-transfer complexes have formed an important category of bifunctional materials over the past two decades.[10] Most commonly, TTF-POM complexes have been synthesized by electrocrystallization, with TTF being oxidized at an anode in the presence of a POM anion. However, in principle, if the POM anions can be designed appropriately, TTF-POM complexes should become

Received: September 20, 2012
Published: November 12, 2012

available by a spontaneous reaction between TTF and POM, analogous to the reaction between TTF and TCNQ. In this study, the vanadium-substituted Keggin-type polyoxometalate $(n\text{-}Bu_4N)_3[SVMo_{11}O_{40}]$, synthesized by the vanadium substitution of the parent POM, $(n\text{-}Bu_4N)_2[SMo_{12}O_{40}]$, provides access to the $V^{V/IV}$ reduction process that lies more positive than the $TTF^{0/+}$ oxidation process.[16−18] Thus, the synthesis of the charge-transfer complex $TTF\text{-}SVMo_{11}O_{40}$ occurs by a rapid and spontaneous reaction between TTF and $(n\text{-}Bu_4N)_3[SVMo_{11}O_{40}]$. A single crystal of this compound was isolated, and the structure was determined by X-ray crystallography. This is the first report of the synthesis and structural characterization of a semiconducting TTF-POM charge-transfer complex prepared by either a solution phase or a solid state spontaneous redox reaction. On the basis of its electrical and magnetic bifunctional properties, this newly isolated TTF-POM material is of interest from both fundamental and applied perspectives.

EXPERIMENTAL SECTION

Materials. Tetrathiafulvalene (TTF, supplied by Aldrich), silver nitrate (Aldrich), ferrocene (Fc, Riedel-de Haën), acetonitrile (MeCN, HPLC grade, Merck), and dichloromethane (CH_2Cl_2, HPLC grade, Merck) were used as received from the manufacturer. Tetrabutylammonium hexafluorophosphate $(n\text{-}Bu_4N)(PF_6)$ was purchased from Wako Pure Chemical Industries and recrystallized from ethanol (95%) before use as the supporting electrolyte in electrochemical experiments. The vanadium substituted polyoxometalate, $(n\text{-}Bu_4N)_3[SVMo_{11}O_{40}]$, was synthesized and purified according to a literature procedure[16] with minor modification. Instead of NH_4VO_3 which was used in the literature procedures, a V(V) stock solution prepared by mixing V_2O_5 and NaOH in water was used in this synthesis. Moreover, concentrated H_2SO_4 was used instead of 2 M H_2SO_4, but the concentrations of V(V) and H_2SO_4 in the mixture of the reactants were set to be the same as reported in the literature.

Voltammetry. Voltammetric experiments were undertaken at 20 ± 2 °C with a Bioanalytical Systems (BAS) 100B electrochemical workstation using a conventional three-electrode cell. Glassy carbon (3 mm in diameter, BAS), gold (1 mm diameter, BAS), and indium tin oxide (ITO)-coated glass (8−12 Ω sq^{-1} sheet resistance, Delta Technologies) disks were used as the working electrodes. The glassy carbon and gold electrodes were polished with 0.3 μm aqueous alumina slurries, rinsed with distilled water and acetone, and then dried with nitrogen gas. The reference electrode was Ag/Ag^+ (10 mM $AgNO_3$, 0.1 M $(n\text{-}Bu_4N)(PF_6)$ in MeCN, −0.078 V vs Fc/Fc^+) while Pt wire was used as the counter electrode. All potentials are reported versus the Ag/Ag^+ reference electrode. All solutions were degassed with the purified nitrogen gas for 10 min prior to electrochemical experiments.

X-ray Crystallography. Data were collected on a single crystal of $TTF_4[SVMo_{11}O_{40}]\cdot 2H_2O\cdot 2CH_2Cl_2$ (prepared as described in the Results and Discussion section) at the Australian Synchrotron using the PX1 beamline operating at 15 KeV (λ = 0.7292 Å). The data collection temperature was maintained at 100 K using an open-flow N_2 cryostream. Initial data processing was carried out using XDS software,[19] and the structure was solved by direct methods with SHELXS-97.[20] Least-squares refinements against F^2 were carried out using SHELXL-97, using the program X-Seed as a graphical interface.[21] All hydrogen atoms were placed in idealized positions and refined using a riding model.

Crystallographic data for $TTF_4[SVMo_{11}O_{40}]\cdot 2H_2O\cdot 2CH_2Cl_2$ are as follows: $C_{26}H_{24}Cl_4Mo_{11}O_{42}S_{17}V$, M = 2801.55, monoclinic, space group $C2/c$ (No. 15), a = 21.699(4) Å, b = 13.883(3) Å, c = 23.120(5) Å, β = 97.98(3)°, V = 6897(2) $Å^3$, Z = 4, D_c = 2.698 g/cm^3, F_{000} = 5364, Mo Kα radiation, λ = 0.7292 Å, T = 100(2) K, $2\theta_{max}$ = 50.0°, 100 519 reflections collected, 6032 unique (R_{int} = 0.0358). Final GOF = 1.052, R1 = 0.0518, wR2 = 0.1266, R indices based on 5978 reflections with $I > 2\sigma(I)$ (refinement on F^2), 484 parameters, 4 restraints. Lp and absorption corrections were applied; μ = 2.821 mm^{-1}. CCDC 838494 contains the supplementary crystallographic data for this paper and can be obtained free of charge from the Cambridge Crystallographic Data Centre via www.ccdc.cam.ac.uk/data_request/cif.

Other Instrumentation and Procedures. Raman (Renishaw RM 2000 Raman spectrograph with 630 nm excitation laser source) and ATR-FTIR (Perkin-Elmer Spectrum 100 instrument with universal ATR sampling accessory) spectroscopies were used for solid state characterization. ^1H NMR spectra were recorded using a Bruker DPX 300 spectrometer. ^1H resonances were referenced to the residual hydrogen from DMSO-d_6 (δ = 2.5 ppm, vs TMS). Scanning electron microscopy (JEOL JSM-7001F FEGSEM) provided the morphological information for electrocrystallized solid samples. Sheet resistance measurements on the solid samples were undertaken with a Jandel RM3-AR four-point probe test meter at 20 ± 2 °C. The thickness was estimated with a Veeco Dektak 150 surface profilometer. Solid samples for resistance measurements were prepared by drop casting a concentrated MeCN suspension of the sample on a piece of microscope glass followed by drying of the sample in a stream of air. The dried pellet was vacuum pressed using a cold isostatic press before its sheet resistance and thickness were measured.

X-band (ca. 9.5 GHz) EPR spectra were recorded with a Bruker ESP380E CW/FT spectrometer. Temperatures between 290 and 110 K were obtained using a standard rectangular TE_{102} cavity together with a Bruker VT2000 temperature controller and associated nitrogen gas flow insert. Lower temperatures between 100 and 2.6 K were obtained using a Bruker ER4118 dielectric resonator inserted in an Oxford Instruments CF935 helium cryostat. Temperatures below 100 K were calibrated against a germanium thermometer using a carbon resistor as a transfer standard. The microwave frequency was measured with an EIP Microwave 548A frequency counter and the g-values were determined by reference to the F^+ line in CaO (g = 2.0001 ± 0.0001).[22] The uncertainty in the g-values is estimated as ±0.001. The experimental spectra were obtained as the first derivative of the absorption, and the spectral intensities were obtained by double integration of the experimental spectrum using the integration routine in the Bruker WINEPR suite. Spectrum simulations were performed using the Bruker XSophe−Sophe−XeprView computer simulation software suite.[23] Magnetic susceptibility measurements were made with sample masses of ∼30 mg using a Quantum Design MPMS 5 SQUID magnetometer in dc magnetic fields of 0.01, 0.10, and 1.0 T. Diamagnetic and other corrections were made as described previously using Pascal's constants and other published data as applicable.[24]

RESULTS AND DISCUSSION

Thermodynamic Data Derived from Cyclic Voltammetry of TTF and $(n\text{-}Bu_4N)_3[SVMo_{11}O_{40}]$ in Acetonitrile. Initially, cyclic voltammograms derived from individual solutions of TTF and $(n\text{-}Bu_4N)_3[SVMo_{11}O_{40}]$ in MeCN solutions (0.1 M $(n\text{-}Bu_4N)(PF_6)$) were obtained. As reported,[24,25] one derived from TTF exhibited two reversible diffusion-controlled, one electron oxidation processes (eqs 1 and 2) with midpoint potentials, E_{m1} = 0.03 V and E_{m2} = 0.41 V (Figure 1). E_m values (all reported versus Ag/Ag^+) were calculated from the average of the oxidation E_p^{ox} and reduction E_p^{red} peak potentials and equate to the reversible formal potentials E_f^0, assuming that the diffusion coefficients for TTF, TTF^+, and TTF^{2+} are identical. In order to achieve the charge transfer material TTF-POM by a spontaneous redox reaction, the $[SV^VMo_{11}O_{40}]^{3-}$ to $[SV^{IV}Mo_{11}O_{40}]^{4-}$ reduction of the polyoxometalate anion must lie between the $TTF^{0/+}$ and $TTF^{+/2+}$ oxidation processes. Polyoxometalate anions often exhibit multiple reversible electron transfer processes, and in MeCN (0.1 M $(n\text{-}Bu_4N)(PF_6)$) solution, $(n\text{-}Bu_4N)_3[SVMo_{11}O_{40}]$ gives rise two well-defined chemically

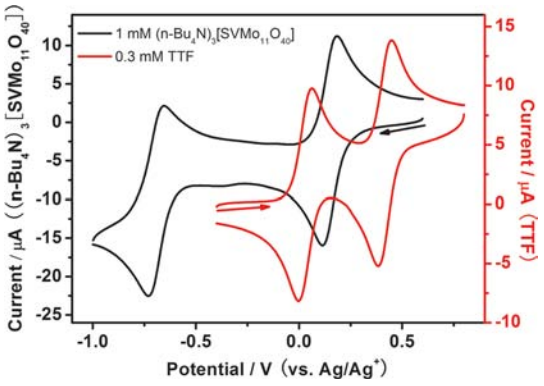

Figure 1. Cyclic voltammograms showing overlap of $TTF^{0/+}$ and $V^{V/IV}$ processes when TTF (0.3 mM) is oxidized and $(n\text{-}Bu_4N)_3[SVMo_{11}O_{40}]$ (1 mM) is reduced in MeCN (0.1 M $(n\text{-}Bu_4N)(PF_6)$). Electrode: glassy carbon (diameter 3 mm). Scan rate = 0.1 V s^{-1}.

reversible one electron reduction processes with E_{m3} = 0.148 V and E_{m4} = −0.692 V (Figure 1, eqs 3 and 4), respectively. Further reduction of this POM occurs at even more negative potentials (Figure S1) but is not discussed in this study, as these processes do not contribute to the chemistry of interest.

According to previous studies of the voltammetry of $[XV^{V}Mo_{11}O_{40}]^{4-}$ (X = P, As) in MeCN[17] and $[SV^{V}Mo_{11}O_{40}]^{3-}$ in mixed MeCN/H_2O solvent,[16] the initial process is assigned to a $V^{V/IV}$ reduction (eq 3), and the second, at more negative potential, is ascribed to the reduction of molybdenum in the POM framework (eq 4).

$$TTF \rightleftharpoons TTF^{+} + e^{-} \quad E_{m1} = 0.03\ V \tag{1}$$

$$TTF^{+} \rightleftharpoons TTF^{2+} + e^{-} \quad E_{m2} = 0.41\ V \tag{2}$$

$$[SV^{V}Mo_{11}O_{40}]^{3-} + e^{-} \rightleftharpoons [SV^{IV}Mo_{11}O_{40}]^{4-} \quad E_{m3} = 0.148\ V \tag{3}$$

$$[SV^{IV}Mo_{11}O_{40}]^{4-} + e^{-} \rightleftharpoons [SV^{IV}Mo_{11}O_{40}]^{5-} \quad E_{m4} = -0.692\ V \tag{4}$$

A minor redox process detected at about −0.34 V is attributed to protonation from adventitious water. Proton sources are known to modify the voltammetry of related systems.[26,27] In summary, the fact that E_{m3} = 0.148 V for the reduction of POM $V^{V/IV}$ lies above the $TTF^{0/+}$ process (E_{m1} = 0.03 V) should allow for a spontaneous redox reaction to occur between TTF_{sol} and $[SV^{V}Mo_{11}O_{40}]^{3-}{}_{sol}$ to give $TTF^{+}{}_{sol}$ and $[SV^{IV}Mo_{11}O_{40}]^{4-}{}_{sol}$ as shown in eq 5. Precipitation then occurs as shown in eq 6.

$$TTF_{sol} + [SV^{V}Mo_{11}O_{40}]^{3-}{}_{sol} \rightleftharpoons TTF^{+}{}_{sol} + [SV^{IV}Mo_{11}O_{40}]^{4-}{}_{sol} \tag{5}$$

$$4\ TTF_{sol} + [SV^{IV}Mo_{11}O_{40}]^{4-}{}_{sol} \rightarrow TTF_4[SV^{IV}Mo_{11}O_{40}]_s \tag{6}$$

Solution Phase Reaction of TTF and $(n\text{-}Bu_4N)_3[SVMo_{11}O_{40}]$. An insoluble TTF-$SVMo_{11}O_{40}$ material was prepared by mixing equimolar $(n\text{-}Bu_4N)_3[SVMo_{11}O_{40}]$ and TTF solutions (both at 1 mM in MeCN). The color of the solution rapidly changed, initially to dark red and then to dark green, and finally a dark brown precipitate was formed. This reaction given in eqs 5 and 6 was allowed to proceed for one hour before the precipitate was collected by centrifugation. The isolated solid material was washed copiously with acetonitrile followed by drying under vacuum to achieve a yield of ∼80% based on TTF. A small amount of this dark solid was then attached to a glass slide for imaging by scanning electron microscopy. The image (Figure 2) reveals the formation of microrods with the average dimensions of 1.5 × 1.5 × 8 μm^3.

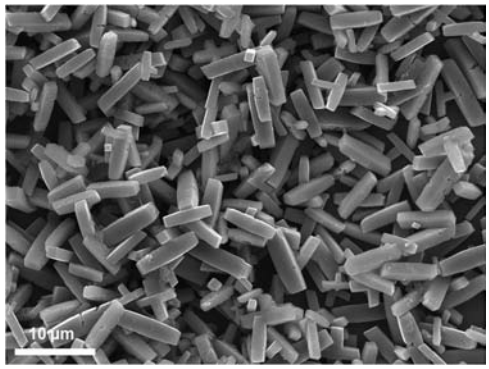

Figure 2. SEM image of the TTF-$SVMo_{11}O_{40}$ material formed by mixing equimolar (1 mM) MeCN solutions of TTF and $(n\text{-}Bu_4N)_3[SVMo_{11}O_{40}]$.

Square wave voltammetry was used to follow the reaction progress by detecting the change in concentration of POM before and after the reaction with TTF. Initially, a voltammogram for 0.5 mM $(n\text{-}Bu_4N)_3[SVMo_{11}O_{40}]$ in MeCN (0.1 M $(n\text{-}Bu_4N)(PF_6)$) was obtained. The peak at −0.69 V shown in Figure 3 is assigned to the second reduction process derived

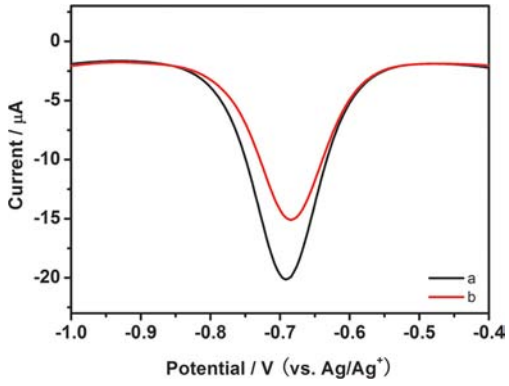

Figure 3. Square wave voltammograms in acetonitrile for (a) 0.5 mM $(n\text{-}Bu_4N)_3[SVMo_{11}O_{40}]$ and (b) the supernatant of the mixture of 0.5 mM TTF and 0.5 mM $(n\text{-}Bu_4N)_3[SVMo_{11}O_{40}]$ containing 0.1 M $(n\text{-}Bu_4N)(PF_6)$ after reaction for overnight. Electrode: 3 mm GCE. Scan rate = 0.1 V s^{-1}.

from dissolved POM (i.e., Mo reduction) which, according to the voltammetric data in Figure 1, should not be influenced by the reaction with TTF. Consequently, the peak current associated with this process can be used to monitor the POM concentration. A 1 mM POM solution was then added to a 1 mM TTF solution in equal volumes to give a mixture that prior to precipitation of solid contained 0.5 mM $(n\text{-}Bu_4N)_3[SVMo_{11}O_{40}]$ and 0.5 mM TTF. The mixture was left to react overnight, to ensure the reaction went to completion. The supernatant solution was collected and subjected to analysis by square wave voltammetry. Comparison with the

dx.doi.org/10.1021/ic302045m | Inorg. Chem. 2012, 51, 12929−12937

original voltammogram of 0.5 mM $(n\text{-}Bu_4N)_3[SVMo_{11}O_{40}]$ revealed that the magnitude for the current from the reduction peak at −0.69 V had decreased to 73% of that found before the reaction with TTF, in good agreement with the value of 75% predicted by eqs 5 and 6.

Reaction between TTF and $(n\text{-}Bu_4N)_3[SVMo_{11}O_{40}]$ in the Solid State. The spontaneous reaction between TTF and $(n\text{-}Bu_4N)_3[SVMo_{11}O_{40}]$, when dissolved into acetonitrile, is predicted on the basis of E_m values. However, it was intriguing to find that a solventless reaction in the solid state also occurred spontaneously between these two reagents. Figure 4 provides

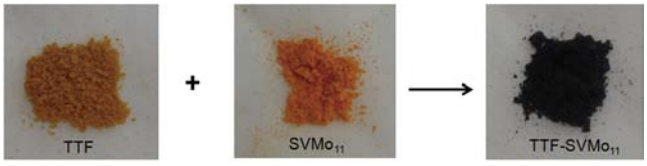

Figure 4. Photographs of TTF, $(n\text{-}Bu_4N)_3[SVMo_{11}O_{40}]$ ($SVMo_{11}$), and a mixture of TTF and $(n\text{-}Bu_4N)_3[SVMo_{11}O_{40}]$ after grinding together for 1 min ($TTF\text{-}SVMo_{11}$).

photographs of an equimolar mixture of TTF_s and $(n\text{-}Bu_4N)_3[SVMo_{11}O_{40}]_s$ ($SVMo_{11s}$) after grinding, showing the rapid changes in color from orange ($SVMo_{11s}$) and yellow (TTF_s) to dark brown ($SVMo_{11}$ + TTF). The solid reaction product was washed with copious amount of acetonitrile, followed by drying under vacuum before being dissolved in DMSO-d_6 and examined by ^1H NMR. The NMR spectrum showed no indication of any $(n\text{-}Bu_4N)^+$ present, as would be expected if $TTF_4[SVMo_{11}O_{40}]_s$ was the only solid present after washing with acetonitrile. That is, no mixed cation TTF^+-$(n\text{-}Bu_4N)^+$ solid was present in the washed solid. In principle, the simplest stoichiometric redox reaction between TTF_s and $(n\text{-}Bu_4N)_3[SVMo_{11}O_{40}]_s$ in the solid state would give $TTF(n\text{-}Bu_4N)_3[SV^{IV}Mo_{11}O_{40}]_s$ as the product. However, rearrangement can produce a 1:3 molar mixture of $TTF_4[SV^{IV}Mo_{11}O_{40}]_s$ and $(n\text{-}Bu_4N)_4[SV^{IV}Mo_{11}O_{40}]_s$ (eq 7) or in general $TTF_x[Bu_4N]_{4-x}[SV^{IV}Mo_{11}O_{40}]$ ($0 < x < 4$). Apparently, $TTF_4[SV^{IV}Mo_{11}O_{40}]_s$ is the least soluble material in acetonitrile, and any $TTF_x[Bu_4N]_{4-x}[SV^{IV}Mo_{11}O_{40}]$ ($0 < x < 4$) compounds formed were removed by washing with acetonitrile, leaving $TTF_4[SV^{IV}Mo_{11}O_{40}]$ as the isolated product. The EPR spectra of the solid derived from either the solution phase reaction or the solid state reaction (after washing with acetonitrile) exhibited the same features, implying that the solids isolated from these two methods are identical.

$$\begin{aligned} TTF_s + (n\text{-}Bu_4N)_3[SV^{V}Mo_{11}O_{40}]_s \\ \rightleftharpoons TTF(n\text{-}Bu_4N)_3[SV^{IV}Mo_{11}O_{40}]_s \\ \rightleftharpoons \frac{1}{4}TTF_4[SV^{IV}Mo_{11}O_{40}]_s \\ + \frac{3}{4}(n\text{-}Bu_4N)_4[SV^{IV}Mo_{11}O_{40}]_s \end{aligned} \quad (7)$$

X-ray Crystallography. Dark crystals of $TTF_4[SVMo_{11}O_{40}]\cdot 2H_2O\cdot 2CH_2Cl_2$ that appeared blue under the microscope were suitable for X-ray crystallographic analysis. These were obtained by layering a solution of $(n\text{-}Bu_4N)_3[SVMo_{11}O_{40}]$ (1 mM in MeCN) over a solution of TTF (2 mM in $MeCN/CH_2Cl_2$, v/v = 4:1). The crystals obtained had the monoclinic space group $C2/c$ with two crystallographically independent TTF^+ moieties, TTF^+-A and TTF^+-B, a half $[SVMo_{11}O_{40}]^{4-}$ anion, and one water and one dichloromethane solvates in the asymmetric unit, as shown in Figure 5a. The crystal structure shows alternating layers of the

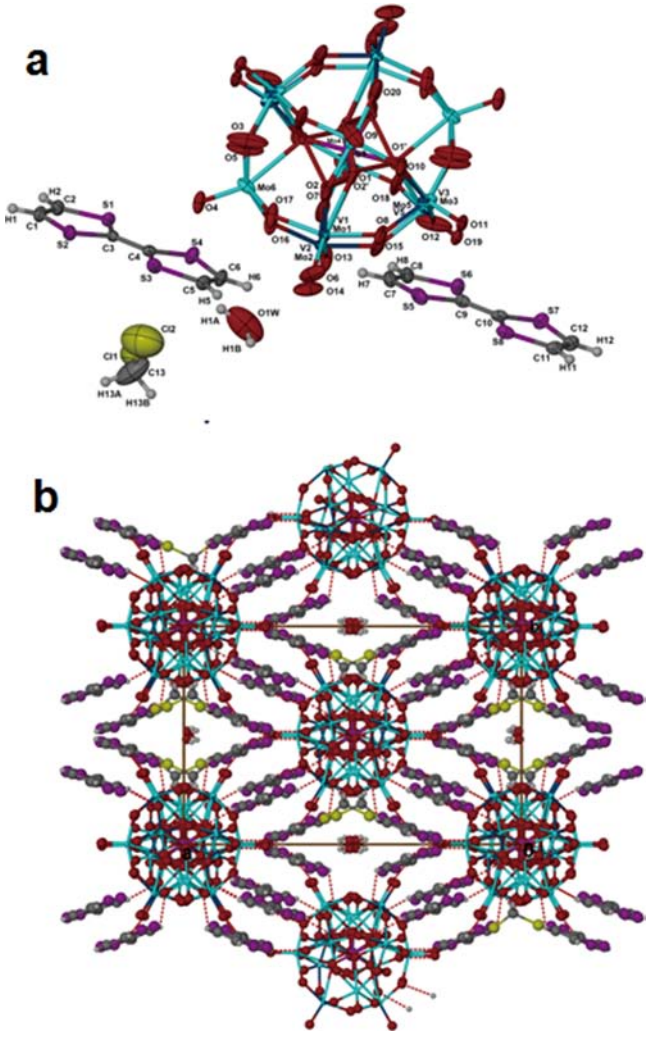

Figure 5. X-ray single crystal structure showing the (a) asymmetric unit for $TTF_4[SVMo_{11}O_{40}]\cdot 2H_2O\cdot 2CH_2Cl_2$ and (b) crystal structure viewed along the c axis. Red dotted line: H-bond interactions between the oxygen atoms of POMs and the CH groups in TTF or CH_2Cl_2 solvate.

α-Keggin-type POM and the TTF moieties (Figure 5b). A noticeable feature in this structure is the locations of Mo and V atoms. Of the six crystallographically independent Mo atoms, two could be refined as Mo atoms (e.g., Mo_4 and Mo_6), whereas the remaining four could only be refined as a mixed Mo/V atom with an occupancy factor being 90% for Mo_1, Mo_3, and Mo_5 and 80% for Mo_2; thus, the vanadium is crystallographically distributed over these four locations with a total 50% atom occupancy in the asymmetric unit cell. This type of disorder has also been observed in the X-ray structure of the reactant polyoxometalate, $(n\text{-}Bu_4N)_3[SVMo_{11}O_{40}]$, where four Mo atoms were refined as a mixed Mo/V atom with a population of 75% for each Mo location.[28]

The reduced $[SV^{IV}Mo_{11}O_{40}]^{4-}$ is a structurally typical α-Keggin polyoxometalate anion, which is formed from 12 MoO_6 octahedra and 1 SO_4 tetrahedron. The central S atom is

dx.doi.org/10.1021/ic302045m | Inorg. Chem. 2012, 51, 12929−12937

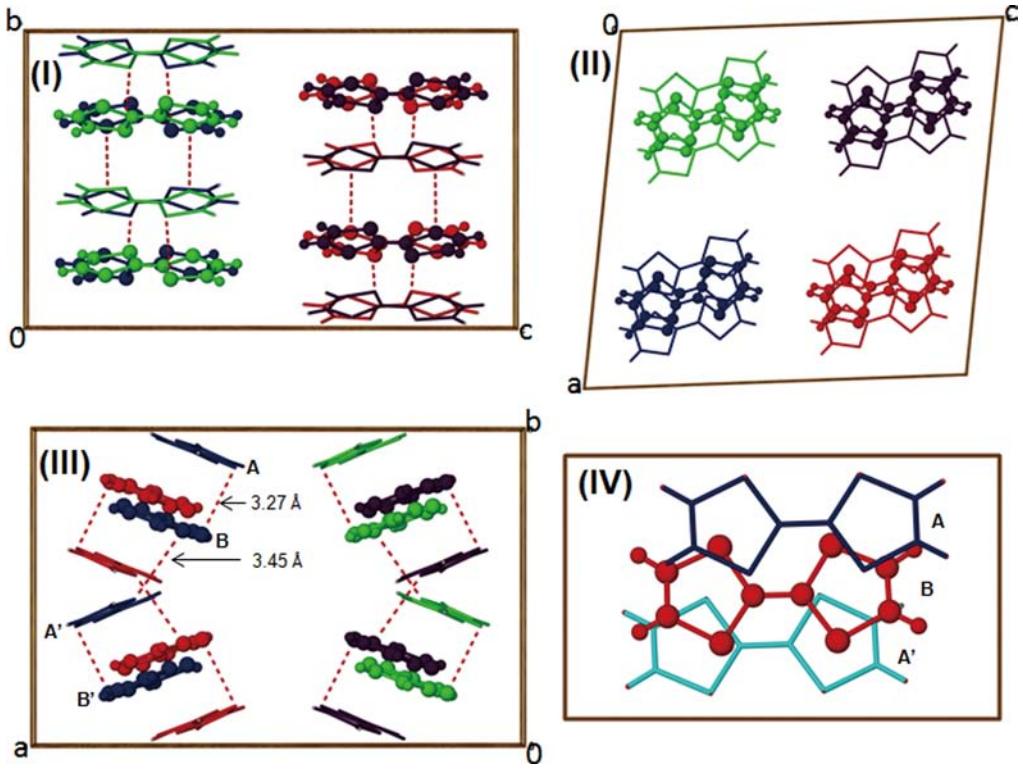

Figure 6. TTF chains of dimers in the $TTF_4[SVMo_{11}O_{40}]$ crystal structure (I) viewed along the *a* axis, (II) viewed along the *b* axis, (III) viewed along the *c* axis, and (IV) showing the diagram of TTF overlap pattern where red, blue, green, and purple colors represent different isolated TTF dimerized chains. Wireframe: TTF-A. Ball: TTF-B.

surrounded by four oxygen atoms with each oxygen site half-occupied. The S−O distances lie in the range 1.404(10)−1.567(8) Å. The Mo−O distances in the α-Keggin cluster can be grouped into three sets, M−O_t (terminal) 1.648(6)-1.664(6) Å, M−O_b (bridge) 1.865(7)−1.947(6) Å, and M−O_c (central) 2.461(9)−2.513(9) Å. In the structure, the donor TTF^+ cations, TTF^+-A and TTF^+-B, are close to planar and lie almost parallel to each other with a dihedral angle of 1.44° between the planes of these two TTF^+ moieties (Figure 6I). The strong S−S interaction between the TTF^+-A and the TTF^+-B links them in stacks of $(TTF)_2^{2+}$ dimers along the *b* axis, with the sequence −ABAB−. The interplanar distance between TTF^+-A and TTF^+-B is 3.27 Å (S1−S8) (Figure 6III) which is considerably shorter than commonly observed in TTF^+ stacks.[29,30] Furthermore, strong S−S interactions are also observed between the adjacent TTF^+ dimers, i.e., TTF^+-B and TTF^+-A′, with the interplanar distance of 3.45 Å (S3−S8) (Figure 6III). Thus, TTF^+ moieties form isolated 1D chains along the *b* axis (Figure 6II) and are separated by the polyoxometalate anions. In addition, the molecules within the TTF^+ dimer are parallel to each other, albeit subtly slipped along the *c* axis and the *a* axis. This is an unusual arrangement of molecular overlapping pattern compared with other reported "ring over central C═C bond" examples, where the TTF-dimers[31−34] are not offset along the *a* axis. A similar overlap pattern also occurs in the adjacent TTF^+ dimers, i.e., TTF-B and TTF-A′ (Figure 6IV).

The degree of charge transfer of the TTF moieties may be estimated using the mean bond lengths of the central C═C and the C—S bonds.[35] Thus, the degrees of charge transfer for TTF-A and TTF-B are identical and agree with the oxidation state of TTF^+ (Table 1). The sum of the charges on the four

Table 1. Degree of Charge Transfer (ρ) Calculated from the Mean Bond Lengths (Å)

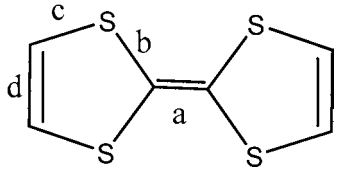

				$TTF_4[SVMo_{11}O_{40}]\cdot 2H_2O\cdot 2CH_2Cl_2$	
bond	TTF[36]	$TTFClO_4$[37]	TTF-TCNQ[38]	TTF-A	TTF-B
a	1.349(3)	1.404(14)	1.369(4)	1.399(4)	1.398(4)
b	1.757(2)	1.713(9)	1.743(4)	1.720(3)	1.720(4)
c	1.726(4)	1.725(11)	1.736(5)	1.727(5)	1.716(2)
d	1.314(3)	1.306(11)	1.323(4)	1.330(3)	1.339(2)
ρ*	0	+1	+0.59	+1	+1

TTF moieties is then estimated as +4 as required for a charge balance with one $[SVMo_{11}O_{40}]^{4-}$ polyoxometalate anionic cluster where the vanadium has been reduced from V(V) to V(IV). Finally, extensive hydrogen bond interactions exist between the oxygen atoms in the $[SVMo_{11}O_{40}]^{4-}$ anion and CH groups in either TTF or the CH_2Cl_2 solvate, which lead to the construction of 2D networks (Figure 5b). The H_2O and CH_2Cl_2 solvates reside within channels between the TTF^+ chains and $[SVMo_{11}O_{40}]^{4-}$ layers (Figure 5b, Table S1).

The TTF-$SVMo_{11}O_{40}$ complex prepared in the solution phase reaction was also subjected to elemental analysis. This complex corresponded to a stoichiometry of $TTF_4[SVMo_{11}O_{40}]\cdot CH_3CN\cdot H_2O$. Calcd: C, 11.71; H, 0.79; N, 0.53; S, 20.42. Found: C, 12.14; H, 0.88; N, 0.67; S, 20.63. The presence of solvated water and acetonitrile was also

dx.doi.org/10.1021/ic302045m | *Inorg. Chem.* 2012, 51, 12929−12937

supported by IR spectra. These data are consistent with the results obtained by X-ray crystallography, with variation in the solvate which is associated with the solvents used to prepare the microcrystalline samples and to grow the single crystals.

Raman Spectroscopy. Raman spectra obtained from $TTF_4[SVMo_{11}O_{40}]$ also were examined in order to probe the redox level of TTF. Since the D_{2h} symmetry of TTF does not change significantly upon oxidation to TTF^+, the same assignments can be used for neutral TTF and TTF^+.[39] The vibrational mode υ_3 (C═C symmetrical stretching) is particularly sensitive to the TTF charge and typically exhibits a large frequency shift upon oxidation.[39−43] The υ_3 frequency shifts from 1515 (in TTF) to 1414 cm^{-1} (in $TTF_4[SVMo_{11}O_{40}]$) in the Raman spectra (Figure S2), consistent with the presence of TTF^+. The doublet at 1553 and 1568 cm^{-1} in TTF also shifts and is found at 1481 and 1503 cm^{-1} in $TTF_4[SVMo_{11}O_{40}]$. These two bands are assigned to the υ_2 fundamental and the combination band of A_g vibrational modes.[39,40]

Electrical and Magnetic Characterizations of the TTF-$SVMo_{11}O_{40}$ Complex. *1. Conductivity.* The sheet resistance of $TTF_4[SVMo_{11}O_{40}]$ for a solid sample prepared by solution phase reaction in acetonitrile was measured using the four point probe method at room temperature (293 ± 2 K). The calculated conductivity for this sample, 1.6×10^{-6} S cm^{-1}, lies within the semiconducting range.

2. Magnetic Susceptibility. The magnetic susceptibility was measured on the $TTF_4[SVMo_{11}O_{40}]$ solid prepared by the solution phase reaction. The temperature dependence of both the susceptibility and the magnetic moment is shown in Figure 7. The temperature dependence of the latter is the more

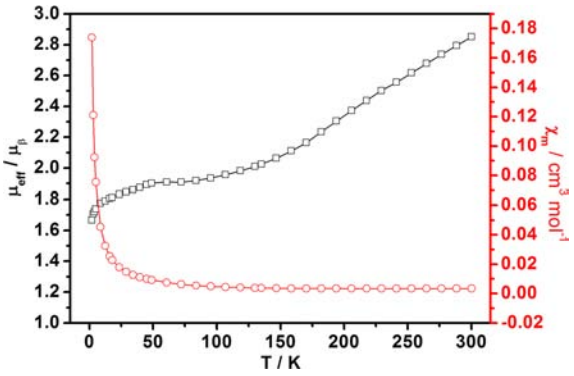

Figure 7. Susceptibility and magnetic moment (μ_{eff}) in Bohr magneton (μ_β) of $TTF_4[SVMo_{11}O_{40}]$ material as a function of temperature at a magnetic field of 1 T.

directly informative as to the number of unpaired spins and here indicates the existence of a multicomponent system with three regions of spin behavior. As shown in Figure 7, the magnetic moment of ~2.0 μ_β at 150 K increases with temperature, reaching ~2.8 μ_β at 300 K.[44] This increase is indicative of the existence of a collection of electron spins coupled by antiferromagnetic interactions with $|J| \gg 300$ K. In the temperature region between 50 and ~150 K, the magnetic moment varies only slightly with temperature with a value of around 1.9 μ_β, consistent with the existence of a spin system with $S = {}^1/_2$ and only one unpaired spin per $TTF_4[SVMo_{11}O_{40}]$ unit. Below ~50 K the magnetic moment decreases. As discussed below, this decrease may be due to antiferromagnetic spin interactions between the V^{4+} ions or as a consequence of the behavior of the $^2T_{2g}$ orbital ground state of this ion. Unlike the case of the TTF-$P_2W_{18}O_{62}$ material described previously,[24] the magnetic moment was essentially independent of the magnetic field (0.001−1.0 T).

3. EPR Spectroscopy. TTF exhibited only a very weak resonance of width 0.96 mT at approximately g = 2.010 associated with the presence of trace amounts of TTF^+. Similarly, polycrystalline $(n\text{-}Bu_4N)_3[SVMo_{11}O_{40}]$ exhibited only very weak resonances due to the parallel and perpendicular components of the 8-line hyperfine spectrum arising from V^{4+} ions (^{51}V; $I = {}^7/_2$; 99.75%). Spectra some 1000 times more intense were obtained at room temperature from the polycrystalline powders obtained by grinding together mixtures of TTF and $(n\text{-}Bu_4N)_3[SVMo_{11}O_{40}]$ in the solid state and by crystallization from a mixture of these two components in a MeCN solution. The strong EPR resonances described below have therefore resulted from the interaction of TTF and the POM in both the solid state and in MeCN solution. The spectra of the solids obtained through crystallization from MeCN solution were more consistent than those of samples obtained by the solid state route. Quantification was further complicated by the sensitivity of the TTF^+ moieties to light and moisture.[45] Nevertheless, the EPR spectral behavior could be correlated in a qualitative fashion with the results of the magnetic susceptibility measurements.

As shown in Figure 8a, the EPR spectrum at 290 K showed the multiline hyperfine resonances expected from V^{4+} and also a

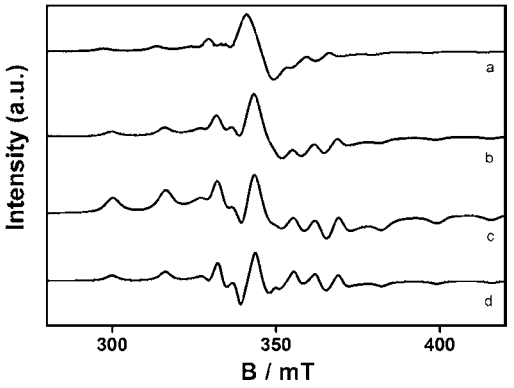

Figure 8. Experimental EPR spectra of $TTF_4[SVMo_{11}O_{40}]$ solid (prepared by the solution phase reaction) at (a) 290, (b) 110, and (c) 2.6 K. (d) Simulation of 2.6 K spectrum. Spectrometer settings: (a−c) receiver gain 1.0×10^4; 100 kHz modulation amplitude 1.0 G; field scan rate 1400 G/84 s; time constant 41s; microwave frequency (a) 9.619 GHz, (b) 9.690 GHz, (c) 9.685 GHz; microwave power (a) 0.105 mW, (b) 4.18 μW, (c) 0.209 μW.

resonance at $g \sim 1.99$ with a width ~8 mT and superimposed on the central resonance of the V^{4+} spectrum. This latter resonance is attributed to unpaired electrons associated with the TTF chains. At 290 K, the intensity of the V^{4+} resonances accounted for all of the V ions present. As the temperature was reduced, the intensity of the $g \sim 1.99$ resonance decreased both absolutely and relative to the V^{4+} resonances (see Figure S3) and, as shown in Figure 8b, was not observed at 110 K. No resonances other than these were observed over the temperature range from 290 K down to 2.6 K in the magnetic field range from 5 to 605 mT, even at spectrometer system gains some 2 orders of magnitude greater than those used for the obtaining spectra of Figure 8.

dx.doi.org/10.1021/ic302045m | Inorg. Chem. 2012, 51, 12929−12937

Table 2. Spin Hamiltonian Parameters Used in the Simulation of the EPR Spectra of $TTF_4[SVMo_{11}O_{40}]$ (Polycrystalline Powder at 2.6 K) and $(n\text{-}Bu_4N)_4[SVMo_{11}O_{40}]$ (Frozen MeCN Solution at 120 K)[a]

	g_x	g_y	g_z	A_x	A_y	A_z	P	α^2
$TTF_4[SVMo_{11}O_{40}]$	1.978	1.978	1.936	53	53	148	0.35	0.80
$(n\text{-}Bu_4N)_4[SVMo_{11}O_{40}]$	1.978	1.978	1.936	53	53	152	0.35	0.84

[a]The components of **A** (^{51}V hyperfine interaction) and **P** (nuclear quadrupole interaction) are in units of $\times 10^{-4}$ cm^{-1}. Uncertainties are as follows: *g*-values ±0.001; **A**-values ±1; **P** ± 0.03. α^2 is the spin density in the $3d_{xy}$ orbital.

The only resonances observed in the temperature range from ~120 K down to 2.6 K were those due to V^{4+}. The 2.6 K spectrum is shown in Figure 8c, and a spectrum simulated using the spin Hamiltonian parameters listed in Table 2 is shown as Figure 8d. No microwave power saturation effects were observed at mW power levels at 2.6 K. As described below, the number of V^{4+} ions contributing to the EPR spectrum decreased below ~50 K although the spectrum itself was essentially unchanged.

The spectra showed that all V^{4+} ion sites are magnetically equivalent, although the X-ray crystallographic evidence is that they are distributed over a number of sites in the polyoxometalate structure. The spin Hamiltonian parameters listed in Table 2 for TTF-$SVMo_{11}O_{40}$ are closely similar to those found for frozen solutions of the electrochemically one-electron reduced $(n\text{-}Bu_4N)_4[SVMo_{11}O_{40}]$ as also listed for comparison purposes in Table 2. These are consistent with those found for the analogous Keggin complexes $(n\text{-}Bu_4N)_4XVMo_{11}O_{40}$ (X = P, As).[17] The *g*- and **A** values are typical for the VO^{2+} ion where the unpaired electron is located in a metal d_{xy} orbital.[46] In the present case, the fractional spin density in the $3d_{xy}$ orbital, calculated using the expressions of McGarvey,[47] is $\alpha^2 = 0.80$, similar to that of the other materials, and indicates that the unpaired electrons are largely localized on the V^{4+} site.

The prominent resonance at $g \sim 1.99$ of width ~8 mT, observed at 290 K, is attributed to unpaired electrons in the TTF chains, where these electrons are sufficiently mobile for the exchange interactions to average out the hyperfine and dipolar interactions. A feature of this resonance was that it decreased in intensity as the temperature was reduced from 290 K toward 110 K and was not observed at lower temperatures. This behavior is consistent with the TTF^+ cations forming a one-dimensional Heisenberg antiferromagnetic chain with a value of $J \gg 300$ cm^{-1}. The decrease in *g*-value from that of the TTF^+ cation can be accounted for by the delocalization of the electronic wave function onto the Mo ions of the polyoxometalate. The fraction of the electron density delocalized onto the polyoxometalate required to give the reduction in *g*-value from the approximate $g = 2.010$ of the TTF cation may be estimated at around 30%.[48]

The temperature dependence of the number of EPR detectable V^{4+} ions is shown in Figure S4 as a plot of $I \times T$ as a function of *T*, where *I* is the EPR absorption intensity (obtained by double integration of the experimental first derivative spectrum) and *T* is the absolute temperature. The data above about 120 K shown in Figure S4 is subject to significant uncertainties, due to the difficulty of subtracting the TTF contribution. However, the quantity $I \times T$ is seen to remain approximately constant until the temperature is reduced to around 50 K, when it commences a decrease to approximately one-third of its high temperature value at 2.6 K. This decrease in the EPR spin concentration below about 50 K occurs at a similar temperature to that of the decrease in magnetic moment shown in Figure 7.

4. Discussion of EPR and Magnetism. The interpretation of the electronic and magnetic properties of $TTF_4[SVMo_{11}O_{40}]$ requires a knowledge of the structural arrangement and the interactions between the organic and inorganic components of the system. The temperature dependence of both the magnetism and the EPR spectra shows three distinguishable regions of behavior. In the temperature range from 300 K down to around 150 K, the magnetic moment decreases, as does the intensity of the resonance at $g \sim 1.99$ attributed to unpaired electrons in the TTF chains. This is consistent with the existence of a one-dimensional Heisenberg antiferromagnetic chain, as may be inferred from the X-ray crystallographic studies at 120 K. These show that the TTF cations form chains of $(TTF)_2^{2+}$ dimers arranged in a stack, where the interplanar spacing of the components of the dimers is 3.27 Å and adjacent dimers are arranged with their planes at an angle of 44.7°, as shown in Figure 6.

In the temperature range from ~120 K down to ~50 K, both the magnetic moment and the V^{4+} EPR intensity vary little as the temperature decreases. The magnetic moment in this temperature range, ~1.9 μ_β, and the EPR intensity imply that there is only one unpaired electron. The spin density, derived from the spin Hamiltonian parameters, show that it is localized in the $3d_{xy}$ orbital of the V^{4+} ions.

In the temperature region below ~50 K, both the magnetic moment and the EPR intensity show a rapid decrease with temperature. Decreases in the magnetic moment with decreasing temperature have been known for V^{4+} complexes for many years[49,50] and are interpreted as being a consequence of the splitting of the $^2T_{2g}$ ground state of the V^{4+} ($3d^1$) ion into orbital singlet and doublet states by spin−orbit coupling and trigonal or tetragonal distortions of the cubic crystal field. Where the splittings between the singlet and doublet states are small, the states are mixed and the magnetic moment is strongly temperature dependent.[51] However, in the present case, the small deviation of the *g*-values from that of g_e, together with the ready observation of V^{4+} resonances at room temperature and the absence of indications of a Jahn−Teller effect at low temperatures, are all consistent with the singlet orbital state being well separated from the doublet by a large axial distortion of the crystal field, as is consistent with expectation for the VO^{2+} ion.

A more likely explanation of the decreases in magnetic moment and EPR detectable spins draws on the similarity with the decreases observed in other salts of π-electron organic donors and inorganic complex anions.[52,53] In some of these cases, a phase change in the TTF chains in the form of a Peierls transition takes place at low temperatures, with a rearrangement into tetrameric structures instead of the dimeric structures observed at the higher temperatures. In the present case, TTF cations are arranged in a 1-D stack and are linked to the POM anions by a three-dimensional network of hydrogen bonds. It

dx.doi.org/10.1021/ic302045m | Inorg. Chem. 2012, 51, 12929−12937

can be speculated that a rearrangement of the TTF cations from a dimeric to a tetrameric arrangement as a result of a Peierls-like transition results in the establishment of pathways for interaction between the electrons on the V^{4+} ions in the POM structure. This interaction would appear to be similar to that proposed for some of the (BEDT-TTF)-polyoxometalate (BEDT-TTF = bis(ethylenedithio)tetrathiafulvalene) complexes described by Coronado et al.[31] where the Keggin anions form a linear chain and antiferromagnetic interactions between substituted metal ions on the surface of the polyoxometalate anions of the chain occur via delocalized electrons. However, we cannot confirm the existence of a Peierls-like transition in the present case, as we were unable to perform the appropriate low temperature conductivity measurements or to determine the structure at liquid helium temperatures.

CONCLUSION

The charge-transfer complex, $TTF_4[SVMo_{11}O_{40}]$, was obtained by spontaneous reaction between TTF and polyoxometalate $(n\text{-}Bu_4N)_3[SVMo_{11}O_{40}]$ in either the solution or solid state phases. X-ray diffraction analysis of a solvated single crystal of this compound indicates a column stacking structure. The Raman spectrum of the solid confirms that the charge on the TTF components is +1, in agreement with results derived from X-ray crystallography. Powdered samples of TTF-$SVMo_{11}O_{40}$ exhibit room-temperature conductivity within the semiconducting range. EPR spectra of this complex at temperatures down to 2.6 K in combination with magnetic data confirm the presence of paramagnetic V(IV) and paramagnetic TTF^+ and also imply the presence of electronic interactions between oxidized TTF and polyoxometalate.

ASSOCIATED CONTENT

Supporting Information

Additional figures and tables. Crystallographic data in CIF format. This material is available free of charge via the Internet at http://pubs.acs.org.

AUTHOR INFORMATION

Corresponding Author

*E-mail: chuji@kochi-u.ac.jp (T.U.), alan.bond@sci.monash.edu.au (A.M.B.).

Notes

The authors declare no competing financial interest.

ACKNOWLEDGMENTS

The authors gratefully acknowledge Dr. B. Moubaraki and Prof. K. S. Murray for magnetic susceptibility measurements. Financial support from the Australian Research Council under the auspices of the Federation Fellowship (AMB) and Discovery Project (LLM, AMB) schemes is acknowledged. We also thank the Australian Synchrotron for the beam time (DAKT, MCJW) and the Monash Centre for Electron Microscopy for assistance in obtaining SEM images.

REFERENCES

(1) Wudl, F.; Smith, G. M.; Hufnagel, E. J. *J. Chem. Soc. D* **1970**, 1453.
(2) Wudl, F.; Wobschall, D.; Hufnagel, E. J. *J. Am. Chem. Soc.* **1972**, *94*, 670.
(3) Coleman, L. B.; Cohen, M. J.; Sandman, D. J.; Yamagish, F. G.; Garito, A. F.; Heeger, A. J. *Solid State Commun.* **1973**, *12*, 1125.
(4) Ferraris, J.; Cowan, D. O.; Walatka, V.; Perlstein, J. H. *J. Am. Chem. Soc.* **1973**, *95*, 948.
(5) Williams, J. M.; Ferraro, J. R.; Thorn, R. J.; Carlson, K. D.; Geiser, U.; Wang, H. H.; Kini, A. M.; Whangbo, M. H. *Organic Superconductors (Including Fullerenes): Synthesis, Structure, Properties, and Theory*; Prentice Hall, Inc.: Englewood Cliffs, NJ, 1992.
(6) Alves, H.; Molinari, A. S.; Xie, H. X.; Morpurgo, A. F. *Nat. Mater.* **2008**, *7*, 574.
(7) Kirtley, J. R.; Mannhart, J. *Nat. Mater.* **2008**, *7*, 520.
(8) Xiao, J. C.; Yin, Z. Y.; Li, H.; Zhang, Q.; Boey, F.; Zhang, H.; Zhang, Q. C. *J. Am. Chem. Soc.* **2010**, *132*, 6926.
(9) Hiraoka, M.; Hasegawa, T.; Yamada, T.; Takahashi, Y.; Horiuchi, S.; Tokura, Y. *Adv. Mater.* **2007**, *19*, 3248.
(10) Coronado, E.; Gimenez-Saiz, C.; Gomez-Garcia, C. J. *Coord. Chem. Rev.* **2005**, *249*, 1776.
(11) Hill, C. L. *Angew. Chem., Int. Ed.* **2004**, *43*, 402.
(12) Long, D. L.; Burkholder, E.; Cronin, L. *Chem. Soc. Rev.* **2007**, *36*, 105.
(13) Mizuno, N.; Misono, M. *Chem. Rev.* **1998**, *98*, 199.
(14) Rhule, J. T.; Hill, C. L.; Judd, D. A. *Chem. Rev.* **1998**, *98*, 327.
(15) Yamase, T. *Chem. Rev.* **1998**, *98*, 307.
(16) Himeno, S.; Osakai, T.; Saito, A.; Hori, T. *Bull. Chem. Soc. Jpn.* **1992**, *65*, 799.
(17) Nambu, J. I.; Ueda, T.; Guo, S. X.; Boas, J. F.; Bond, A. M. *Dalton Trans.* **2010**, *39*, 7364.
(18) Himeno, S.; Takamoto, M.; Hoshiba, M.; Higuchi, A.; Hashimoto, M. *Bull. Chem. Soc. Jpn.* **2004**, *77*, 519.
(19) Kabsch, W. *J. Appl. Crystallogr.* **1993**, *26*, 795.
(20) Sheldrick, G. M. *Acta Crystallogr., Sect. A* **2008**, *64*, 112.
(21) Barbour, L. J. *J. Supramol. Chem.* **2001**, *1*, 189.
(22) Wertz, J. E.; Orton, J. W.; Auzins, P. *Discuss. Faraday Soc.* **1961**, *31*, 140.
(23) Hanson, G. R.; Gates, K. E.; Noble, C. J.; Griffin, M.; Mitchell, A.; Benson, S. *J. Inorg. Biochem.* **2004**, *98*, 903.
(24) Li, Q.; Zhao, C.; Bond, A. M.; Boas, J. F.; Wedd, A. G.; Moubaraki, B.; Murray, K. S. *J. Mater. Chem.* **2011**, *21*, 5398.
(25) Shaw, S. J.; Marken, F.; Bond, A. M. *Electroanalysis* **1996**, *8*, 732.
(26) Vu, T.; Bond, A. M.; Hockless, D. C. R.; Moubaraki, B.; Murray, K. S.; Lazarev, G.; Wedd, A. G. *Inorg. Chem.* **2001**, *40*, 65.
(27) Bond, A. M.; Coomber, D. C.; Harika, R.; Hultgren, V. M.; Rooney, M. B.; Vu, T.; Wedd, A. G. *Electroanalysis* **2001**, *13*, 1475.
(28) See crystal structure of $(n\text{-}Bu4N)_3[SVMo_{11}O_{40}]$, CCDC 840579.
(29) Triki, S.; Ouahab, L.; Grandjean, D. *Acta Crystallogr., Sect. C* **1993**, *49*, 132.
(30) Triki, S.; Ouahab, L.; Padiou, J.; Grandjean, D. *J. Chem. Soc., Chem. Commun.* **1989**, 1068.
(31) Coronado, E.; Galán-Mascarós, J. R.; Giménez-Saiz, C.; Gómez-García, C. J.; Triki, S. *J. Am. Chem. Soc.* **1998**, *120*, 4671.
(32) Phillips, T. E.; Kistenmacher, T. J.; Ferraris, J. P.; Cowan, D. O. *J. Chem. Soc., Chem. Commun.* **1973**, 471.
(33) Takahashi, K.; Shirahata, T.; Tomitani, K. *J. Mater. Chem.* **1997**, *7*, 2375.
(34) Gómez-García, C. J.; Coronado, E.; Triki, S.; Ouahab, L.; Delhaes, P. *Adv. Mater.* **1993**, *5*, 283.
(35) Ouahab, L.; Fettouhi, M.; Halet, J. F.; Yartsev, V. M.; Garrigoulagrange, C.; Delhaes, P.; Sourisseau, C. *New J. Chem.* **1993**, *17*, 399.
(36) Cooper, W. F.; Kenny, N. C.; Edmonds, J. W.; Nagel, A.; Wudl, F.; Coppens, P. *J. Chem. Soc. D* **1971**, *16*, 889.
(37) Yakushi, K.; Nishimura, S.; Sugano, T.; Kuroda, H.; Ikemoto, I. *Acta Crystallogr., Sect. B* **1980**, *36*, 358.
(38) Kistenmacher, T. J.; Phillips, T. E.; Cowan, D. O. *Acta Crystallogr., Sect. B* **1974**, *30*, 763.
(39) Van Duyne, R. P.; Cape, T. W.; Suchanski, M. R.; Siedle, A. R. *J. Phys. Chem.* **1986**, *90*, 739.
(40) Bozio, R.; Girlando, A.; Pecile, D. *Chem. Phys. Lett.* **1977**, *52*, 503.

(41) Bozio, R.; Zanon, I.; Girlando, A.; Pecile, C. *J. Chem. Phys.* **1979**, *71*, 2282.
(42) Berlinsky, A. J.; Hoyano, Y.; Weiler, L. *Chem. Phys. Lett.* **1977**, *45*, 419.
(43) Siedle, A. R.; Candela, G. A.; Finnegan, T. F.; Van Duyne, R. P.; Cape, T.; Kokoszka, G. F.; Woyciejes, P. M.; Hashmall, J. A. *Inorg. Chem.* **1981**, *20*, 2635.
(44) The magnetic moment of a spin system, μ_{eff}, is derived from a measurement of the susceptibility, χ, where χ is proportional to $(\mu_{eff})^2$. Thus, while the total susceptibility of two independent spin systems is measured as $\chi_1 + \chi_2$, the magnetic moment of the combined system is $[c_1(\mu_{1eff})^2 + c_2(\mu_{2eff})^2]^{1/2}$, where c_1 and c_2 are proportionality constants. For example, the magnetic moment of two independent spin systems each with $S = {}^1/_2$ and $g = 2$ is $\sim$ 2.45 Bohr magnetons and not $\sim$2.83 μ_β, as is the case for a $S = 1$ system of two coupled spins of $S = {}^1/_2$.
(45) TTF^+ radical is not stable when illuminated with white light or natural light when water is present.
(46) Kivelson, D.; Lee, S. *J. Chem. Phys.* **1964**, *41*, 1896.
(47) McGarvey, B. R. *J. Phys. Chem.* **1967**, *71*, 51.
(48) Resonances with *g*-values intermediate between those of an organic radical and an isolated paramagnetic ion in a cluster have been observed by, e.g., Penicaud et al.: Penicaud, A.; Batail, P.; Perrin, C.; Coulon, C.; Parkin, S. S. P.; Torrance, J. B. *J. Chem. Soc., Chem. Commun.* **1987**, 330. The *g*-value of such a system is given by $g = g_r\alpha + g_m(1 - \alpha)$, where g_r and g_m are the *g*-values of the radical and the magnetic ion in the cluster, respectively, and α is the electron density on the radical. See: Tomkiewicz, Y.; Taranko, A. R.; Torrance, J. B. *Phys. Rev. Lett.* **1976**, *36*, 751. For the present purposes, we use the *g*-value of the TTF radical of $\sim$ 2.010. See: Walsh, W. M.; Rupp, L. W.; Wudl, F.; Kaplan, M. L.; Schafer, D. E.; Thomas, G. A.; Gemmer, R. *Solid State Commun.* **1980**, *33*, 413. The value of Mo^{5+} ions in the Mo_{12} Keggin cluster is $\sim$1.945. See: Prados, R. A.; Pope, M. T. *Inorg. Chem.* **1976**, *15*, 2547.
(49) Figgis, B. N. *Trans. Faraday Soc.* **1961**, *57*, 198.
(50) Machin, D. J.; Murray, K. S. *J. Chem. Soc. A* **1967**, 1330.
(51) Dunbar, K. R.; Schelter, E. J.; Tsukerblat, B. S.; Ostrovsky, S. M.; Mirovitsky, V. Y.; Palii, A. V. *Polyhedron* **2003**, *22*, 2545.
(52) Dumm, M.; Loidl, A.; Fravel, B. W.; Starkey, K. P.; Montgomery, L. K.; Dressel, M. *Phys. Rev. B* **2000**, *61*, 511.
(53) Coronado, E.; Clemente-León, M.; Galán-Mascarós, J. R.; Giménez-Saiz, C.; Gómez-García, C. J.; Martínez-Ferrero, E. *J. Chem. Soc., Dalton Trans.* **2000**, 3955.